Langmuir

Article

pubs.acs.org/Langmuir

Enveloping Self-Assembly of Carbon Nanotubes at Copolymer Micelle Cores

Matthias M. L. Arras,[†] Christoph Schillai,[†] and Klaus D. Jandt*[,†,‡]

[†]Chair of Materials Science, Department of Materials Science and Technology, Otto Schott Institute of Materials Research, Faculty of Physics and Astronomy, Friedrich Schiller University Jena, Löbdergraben 32, 07743 Jena, Germany

[‡]Jena Center for Soft Matter (JCSM), Friedrich Schiller University Jena, Humboldtstraße 10, 07743 Jena, Germany

Supporting Information

ABSTRACT: Carbon nanotubes (CNTs) and their polymer nanocomposites are interesting materials for future applications, for example in optics or electronics. Research faces two major challenges with these outstanding nanofillers: control over dispersion and spatial arrangement within the nanocomposite, both required to achieve optimal structure and properties of CNT-based nanocomposites. We report on novel self-assembled multiwall CNT (MWCNT)/block copolymer (BCP) nanostructures realized by patterning MWCNTs with amphilphilic diblock copolymer micelles. A high molecular weight poly(styrene)-*b*-poly(2-vinylpyridine) BCP which forms large micelles (250 nm) was chosen to facilitate the templating by reducing the bending energy induced in the MWCNTs. We tested the hypothesis that it is possible to use an amphiphilic BCP as a dispersing agent and its spherical micelles as a template at the same time without modification of the CNTs. In thin films of the MWCNT/BCP micelles, highly separated MWCNTs were repeatedly observed which enveloped the core of the BCP micelles, i.e., the *unfunctionalized* MWCNTs segregated to the interface between the two BCP phases. Depending on the size of the MWCNTs, ring-like (split-ring) or network forming structures were obtained. The MWCNT templating mechanism, i.e., the segregation to the interface, is explained by the interfacial tension within the BCP interface and the chain entropy. The reported new complex nanocomposite has potential to be applied for example as cost-effective split-ring resonators for metamaterials or for conductive polymer films with an extremely low percolation threshold.

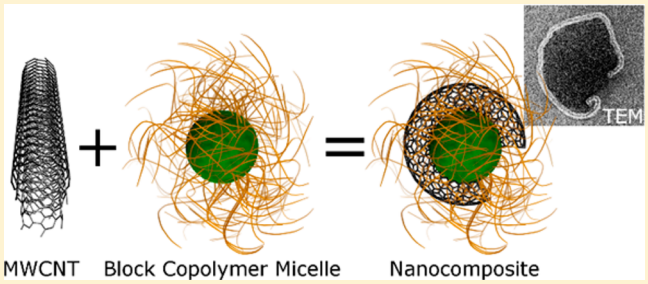

INTRODUCTION

Carbon nanotubes (CNTs) are ideal nanofillers for composites and are applied in mechanically reinforced polymer nanocomposites,[1] in photovoltaics,[2] and as sensors,[3] actuators,[4] and transistors.[5]

In many cases, a prerequisite for the effective application of CNTs is their stable and homogeneous dispersion within the respective matrix because agglomeration cancels at least some of the benefits of its nano dimension.

A stable CNT dispersion can be generally accomplished by covalent modification of the CNTs[6] or the use of ionic or specific interactive dispersants.[7] Both approaches negatively influence the mechanical integrity and electronic properties of CNTs nanocomposites.[8] An alternative approach to achieve stable dispersion without those limitations is the direct use of amphiphilic copolymers as the matrix phase. It has been shown that amphiphilic block copolymers (BCPs) in selective solvents adsorb on CNTs as individual chains,[9] as encapsulating monolayer,[10,11] or as micelles[12,13] which debundle CNTs and stabilize CNT dispersions in solution.

Because of the inherent CNT anisotropy, the control of the CNT spatial distribution and orientation within the matrix is key to exploiting their outstanding properties on a macroscopic scale. Significant progress has been made on the alignment of CNTs in CNT/polymer composites.[14,15] It is still challenging to control the CNT arrangement on an individual CNT level, e.g., to control the intertube ordering and spatial distribution of CNTs in nanocomposites or even more complex arrangements over a macroscopic region.

Recently, scientists started to use microphase separation induced nanostructures of BCPs to template *functionalized* CNTs,[16−18] i.e., guiding the CNTs to segregate to one of the BCPs domains by rendering it chemically compatible to that domain. Yet, to the best knowledge of the authors, there has been no report on the possibility to use the BCP as a CNT dispersant and as a templating tool at the same time.

Here, we introduce that large BCP micelles can template *unfunctionalized* CNTs and show that the good CNT dispersing properties of BCPs can be combined with the ability of BCP micelles at the same time to realize new CNT/polymer nanostructures. As presented in this paper, here, the templating will be due to the reduction in surface tension between the two

Received: June 12, 2014
Revised: October 6, 2014
Published: October 31, 2014

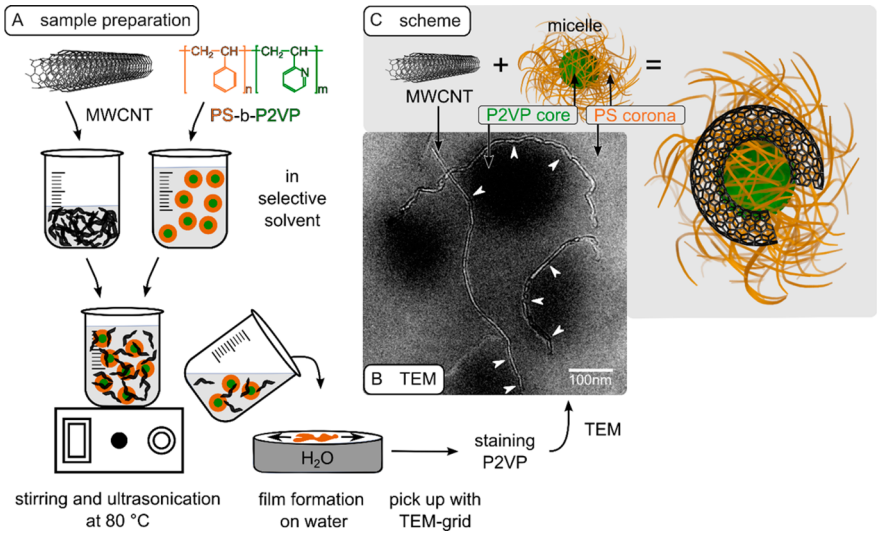

Figure 1. MWCNT/BCP micelle nanostructure. (A) MWCNT/BCP micelle thin film preparation process and (B) a corresponding transmission electron microscopy (TEM) micrograph of the stained film. The micelles' P2VP cores are stained dark while the micelles' PS coronas stay light. The arrows indicate the MWCNT envelopment. (C) The individual MWCNTs envelop the micelle's core as shown in the schematic depiction. Except for (B), sizes not true to scale and images are schematic.

BCP phases by the CNT. To this end, we created a solution of multiwall CNTs (MWCNTs) and a high molecular weight amphiphilic BCP poly(styrene)-*block*-poly(2-vinylpyridine) (PS-*b*-P2VP) which formed micelles in a selective solvent and we investigated its uncompressed Langmuir films (see Figure 1A).

EXPERIMENTAL SECTION

Materials. PS-*b*-P2VP was purchased from Polymer Source Inc., Dorval, Canada (M_{PS} = 380 kg mol^{-1} and M_{P2VP} = 129 kg mol^{-1}) and synthesis grade *p*-xylene from Merck (Darmstadt, Germany). Short and thin MWCNTs (catalytic carbon vapor deposition, 9.5 nm × 1 μm according to specifications) were obtained from Sigma-Aldrich (Taufkirchen, Germany). All materials were used as received.

Langmuir Film Preparation. 0.25 wt % MWCNTs in *p*-xylene were dispersed in an ultrasonicator for 40 min at 80 °C (VWR ultrasonic cleaner USC 300TK, 45 kHz, 80 W). A 0.25 wt % solution of PS-*b*-P2VP in *p*-xylene was stirred for 20 min at 120 °C and slowly added to the MWCNTs in the ultrasonicator at 80 °C. The final weight ratio of MWCNTs and PS-*b*-P2VP in the solution was 1:3. The Langmuir films were prepared by spreading 45 μL of the MWCNT/BCP solution on Millipore water in a 7 cm wide Petri dish at room temperature.

Transmission Electron Microscopy. The dried film was then transferred from the water surface to platinized transmission electron microscopy (TEM) grids by the Langmuir–Schaefer technique, stained in iodine vapor for 4.5 h and examined with a JEOL 3010 TEM (JEOL, Eching, Germany) at an accelerating voltage of 300 kV. In addition, drop-casting of 0.25 wt % PS-*b*-P2VP only solution on carbon-coated TEM grids was performed with the same staining conditions and subsequently pictured in the TEM. TEM images were contrast enhanced (ImageJ 1.48q) and flattened (Gwyddion 2.31); in addition, individual MWCNTs were highlighted manually by dodging (Gimp 2.8.10). The unmodified micrographs of the TEM micrographs presented in the paper are enclosed in the Supporting Information.

Atomic Force Microscopy and Dynamic Light Scattering. For atomic force microscopy (AFM) (Dimension 3100, Digital Instruments, Santa Barbara, USA) investigations, the film was transferred to mica by the Langmuir–Schaefer technique. The micelle size distribution was measured by dynamic light scattering (DLS) (Zetasizer, Malvern Instruments, Malvern, UK) at room temperature in *p*-xylene.

RESULTS AND DISCUSSION

The nanostructure of this MWCNT/BCP micelle thin film was analyzed in the TEM which is shown in Figure 1B (see Supporting Information for additional TEM micrographs). The thin film consisted of bent MWCNTs and loosely packed, large BCP micelles. The PS-*b*-P2VP micelle, in turn, was composed of a P2VP core which had been stained dark and was surrounded by a PS corona (unstained, i.e., light).

The overall mean micelle size of the BCP only was $d_{micelle}$ = 250 nm (determined by DLS, see Figure 2A). The average micelle's core diameter after drop-casting on a carbon-coated copper grid was approximately d_{core} = 80 nm (determined by TEM, see Figure 2B). Using 10-fold lower BCP concentrations yielded the same micelle size distribution (see Supporting Information), suggesting that the micelles forming in this study were thermodynamically stable (spherical micelles and no colloidal aggregates).

In comparison, when using the Langmuir–Schaefer technique as described above, the micelle core size increased to approximately d_{core} = 150 nm (determined by TEM, see Figure 2C). In addition to the TEM images, AFM was used to analyze the micelle thin film surface. For the MWCNT/BCP micelle thin film, protruding micelle cores and MWCNTs were found on the film side of the former film–water interface which is shown in Figure 3A.

The film thickness in the corona region as measured at line defects of the film ranged from approximately 50-100 nm. Thus, the large spherical BCP micelles may have spread and deformed on the water surface after drop casting because the corona is hydrophobic and the core is hydrophilic. This explains the difference in micelle size when using direct drop casting versus the Langmuir–Schaefer technique (see Figure 2B,C). The thin film's air–film interface was irregular, and no MWCNTs were found on the surface (see Supporting Information). Based on the AFM images, a simple model of the film's cross-section was devised and is shown in Figure 3B.

The micellization of amphiphilic BCPs[19,20] and their Langmuir films has been studied previously in detail.[21,22] In principle, it is possible to fabricate regularly, highly ordered

dx.doi.org/10.1021/la502298j | *Langmuir* 2014, 30, 14263–14269

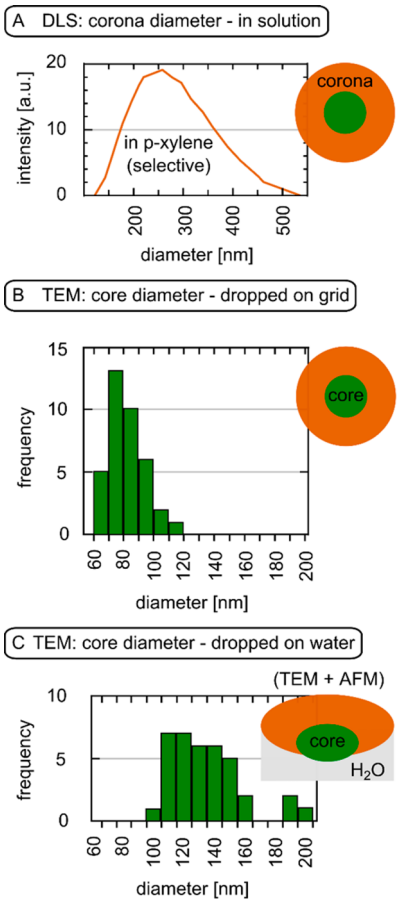

Figure 2. Size characterization of micelles under different conditions. (A) Dynamic light scattering (DSC) determined hydrodynamic radius of micelle corona. Micelle core diameter after (B) drop-casting directly on carbon-coated TEM grid and (C) after dropping on water and subsequent retrieval. In conjunction with atomic force microscopy (AFM) height images (see Figure 3), this suggests that the micelles spread on the water surface. Schemes not drawn true to scale.

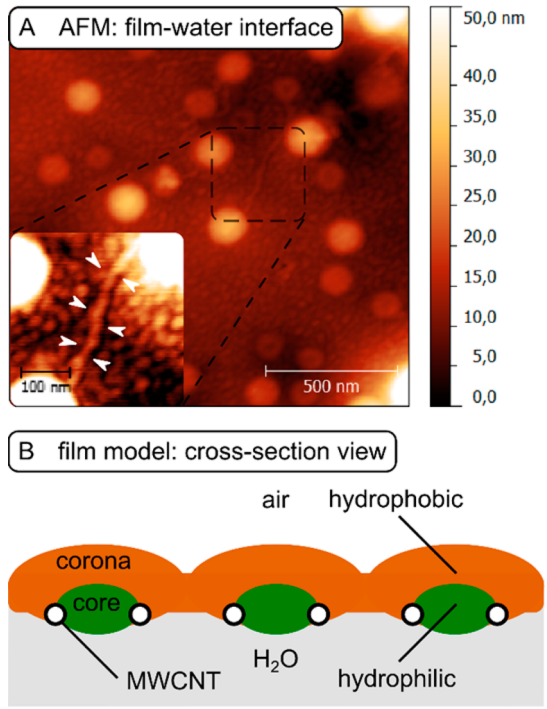

Figure 3. MWCNT/BCP micelle thin film. (A) Atomic force microscopy (AFM) height image of the MWCNT/BCP micelle thin film with the former film–water interface facing up (measured in air, dried film). The arrows in the inset exemplarily highlight a MWCNT which is visible in the vicinity of the film–water interface. (B) A corresponding model of the MWCNT/BCP micelle thin film's cross section with the micelles' cores protruding out of the film plane created on water. Not drawn true to scale.

close-packed micelles using a Langmuir–Blodgett trough.[21] Since in our experiment the BCP micelles size distribution was not monodisperse (see Figure 2) and their Langmuir film was uncompressed, the micelle order within the MWCNT/BCP micelle thin film was low.

The most interesting feature of the MWCNT/BCP micelle thin film, however, was revealed by the TEM: The MWCNTs were not regularly distributed over the entire film but rather distinctly enveloped the micelles' cores (Figure 1B). A schematic picture of this novel MWCNT/BCP nanostructure is presented in Figure 1C. Despite their high Young's modulus and the associated bending energy under deformation, CNTs have been shown to be bendable to a high degree.[23,24]

In Figure 4A, a stitched montage of individual TEM images is presented. The dispersion of individual MWCNTs is very high as can be seen in the figure. This high degree of MWCNT dispersion is representative for the whole sample, although sporadically some small MWCNT agglomerates were found (see Supporting Information). This agrees with previous studies which observed well dispersed CNTs in amphiphilic copolymers solutions.[12,13]

The MWCNTs frequently follow the contour of the BCP micelles' core–corona interface, even when a substantial degree of MWCNT bending is necessary (white arrows in Figure 4A). Therefore, we propose that the majority of MWCNTs distinctively segregate to the interface of the PS-*b*-P2VP micelles.

To provide statistical data for the specific MWCNT segregation to the micelle core–corona interface, the MWCNT location distribution was obtained by image analysis (see Supporting Information for details). To this end, the TEM images (see Figure 4A) were segmented into three regions: corona, interface, and core. For each of the three regions, the MWCNT density, i.e., the overall MWCNT area in the region per total area of the respective region, was calculated. The results are shown in Figure 4B. The MWCNT density in the interface region was more than a factor of 2 higher than for the other regions. Thus, the proposed preferred MWCNT segregation to the micelle's core–corona interface was confirmed.

Depending on the length of the MWCNTs in relation to the micelles' diameter, the resulting MWCNT/BCP nanostructure was different. Rings and split-ring structures were present for short MWCNTs (Figure 5A, first row). Longer MWCNTs formed networks by linking more than one micelle (Figure 5A, second and third row). It is assumed that the MWCNT segregation to multiple micelles partially prevented the MWCNTs from enveloping one micelle core entirely. The maximum number of cores a single MWCNT interacted with was three (average MWCNT length used was 1 μm, average micelle diameter 250 nm).

Furthermore, that MWCNT bend around *multiple* BCP micelles' cores explains the remaining high values for the MWCNT density in the corona: MWCNTs interfacing with

dx.doi.org/10.1021/la502298j | *Langmuir* 2014, 30, 14263–14269

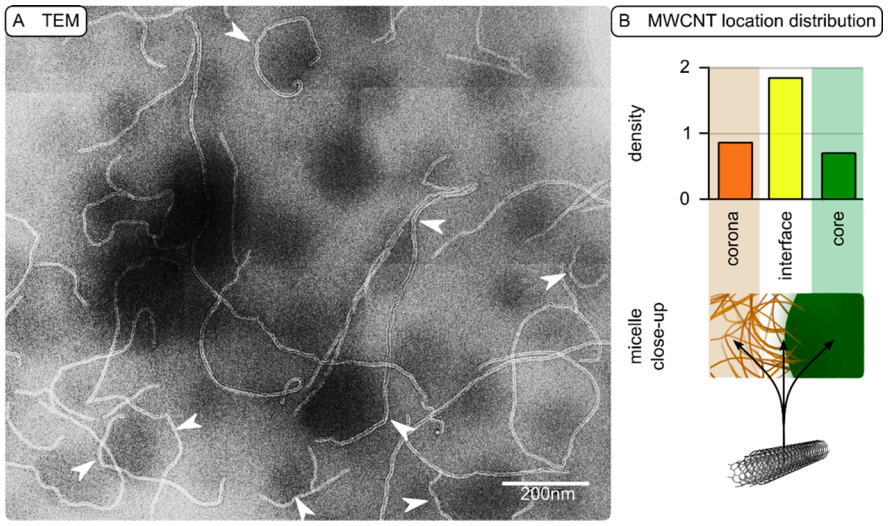

Figure 4. Distribution of MWCNTs over the MWCNT/BCP micelle thin film. (A) Large area TEM micrograph (individual, stitched pictures) revealing that MWCNTs segregate to the micelles' core−corona interface. The white arrows point to MWCNTs which follow the core−corona interface of one or more BCP micelles, even when a substantial bending of the MWCNT is involved. Note the high level of MWCNT dispersion. (B) The corresponding MWCNT location distribution showing the MWCNT density in the three regions of the BCP micelles film: corona, interface, and core.

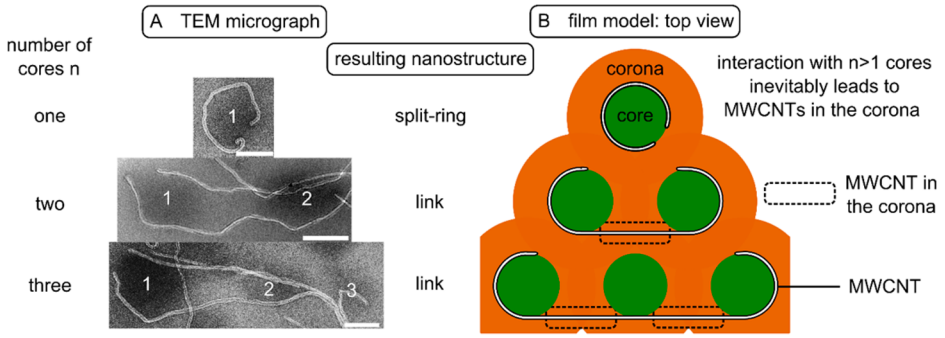

Figure 5. List of nanostructures obtained by templating MWCNTs of different length: MWCNTs envelop one to three micelles. (A) TEM micrographs of representative nanostructures. The scale bar in the TEM images is 100 nm in each case. (B) Corresponding model of the film in top view.

more than one core must inevitably cross the corona (Figure 5B).

An important aim of CNT composite research is the fabrication of straight and aligned CNTs and their composites.[14,25] Nevertheless, researchers aim to create more complex arrangements for new nanomaterials applications. For example, closed ring CNT structures have already been obtained[23,26,27] but not within a CNT/polymer composite. The stability of closed ring structures presented in the literature arises from chemical binding of the CNT ends.

In the present MWCNT/BCP nanocomposite, the BCP micelle templated MWCNT ring structures are often open, which renders them useful for potential applications in optical metamaterials:[28,29] The open MWCNT ring resembles a split-ring resonator which is a common building block of metamaterials because it can interact with electromagnetic waves.[28] Since a matrix phase is necessary to stabilize the split-ring structure, the CNT split-ring structure is unique to the present study and has not previously been observed in studies on CNT ring formation. Furthermore, the ability to allocate the MWCNT to a very narrow region, i.e., the BCP interface, will allow for a percolated conducting network with an extremely low percolation threshold.[30] For electrical conducting CNT networks the use of *unfunctionalized* CNTs is benefitial as the electronic properties are not altered and the surfactant does not additionally increase the tunnel resistance between the individual CNTs. In addition, the P2VP block of the used BCP phase can be used to selectively nucleate metallic nanoparticles which still increase the number of possible applications for the present MWCNT/BCP nanocomposite.[31]

So far, CNT/BCP nanocomposites which exploit the BCP microphase separation for the spatial control of single CNTs have only been realized for *functionalized* CNTs. The predominantly reported *functionalized* MWCNT/BCP nanostructure comprise of CNTs which are located in the center of the, to the chemical functionalization corresponding, copolymer's phase.[16,18] This is a major contrast to the MWCNT/BCP core−corona interface affinity reported here for *unfunctionalized* MWCNTs.

The bending energy which is required to bend a MWCNT around a micelle's core with a diameter of d_{core} = 150 nm in the present study is estimated to be approximately 2×10^{-8} J/m (see Supporting Information for estimation). For example, for a 500 nm long MWCNT this yields 10 fJ. Thus, substantial energy is necessary to envelop the BCP micelle cores by MWCNT, and any possible mechanism must be able to explain

dx.doi.org/10.1021/la502298j | *Langmuir* 2014, 30, 14263−14269

the origin of this energy. Although it cannot be ruled out that possible initial defects within the MWCNTs helped to accommodate the micelles' shape, we propose that the major bending energy originated from the BCP core−corona interface.

The important role of the BCP interface for nanotemplating has already been observed for nanoparticle/BCP systems. Bockstaller et al.[32] found that *functionalized* nanoparticles segregate to specific regions depending on their size: smaller ones migrate into the interface between the two phases of the BCP, while larger particles migrate to the central region of the corresponding phase (small in terms of the BCP domain size). This behavior has been predicted in simulations earlier.[33] Li et al.[17] suggested that PEO-*functionalized* MWCNT may not always segregate to the center of the corresponding PEO phase of a PS-*b*-poly(ethylene oxide) BCP but may also be found in the PS-phase in the vicinity of the interface.

Yet, there are no specific theoretical calculations for the segregation of CNTs in nanostructured copolymers, but those are available for a similar system: the nanorod/copolymer nanocomposite. In these studies, it has been found that under certain conditions long *unfunctionalized* nanorods segregate to the interface of a diblock copolymer.[34] The behavior of *unfunctionalized* nanofillers has been proven for nanoparticles where it was found that only nanoparticles which have no affinity for either of the blocks segregate to the interface of the BCP.[35]

In the case of thermodynamic equilibrium, the specific MWCNT segregation to the BCP interface can be explained by considering the energy in an A−B diblock copolymer interface $E_{A,B}$. Since the radius of micelles is large, it is sufficient to consider $E_{A,B}$ for a simple lamellar BCP which is[36]

$$E_{A,B} = \gamma_{A,B}\Sigma + \frac{\frac{3}{2}k_bT\left(\frac{\lambda}{2}\right)^2}{Nl^2} \quad (1)$$

It is a consequence of two contributions: the interfacial tension $\gamma_{A,B}$ and the entropic chain stretching energy which is mainly a function of the lamellar thickness λ and the effective chain segment length l (for a definition of the other terms see Supporting Information). The chain stretching is due to the chemical incompatibility of both blocks, which are yet covalently bonded. To minimize the mutual mer A−mer B contact, the polymer chains deviate from the random coil morphology and stretch out in the interface region. The chain stretching is a general and important principle found in BCPs and is the origin of the variety of microphase separated structures which these polymers can form.[36]

The interfacial tension of two polymers $\gamma_{A,B}$ can be linked to the absolute value of the Hildebrand solubility parameter difference (see Supporting Information for derivation of eq 2 and comment on the use of Hildebrand solubility parameters instead of Hansen solubility parameters):

$$\gamma_{A,B} \sim |\delta_A - \delta_B| \quad (2)$$

Table 1 shows the Hildebrand solubility parameter for the relevant materials and derived quantities according to eq 2.

The solubility parameter of the CNT lies roughly in the middle of the respective polymer values. Therefore, according to eq 1, the energy in the BCP interface will be lowered by the MWCNT segregation to this interface because the effective interfacial tension is reduced ($|\delta_{CNT} - \delta_{polymer}| < |\delta_{PS} - \delta_{P2VP}|$ and, thus, $\gamma_{CNT,polymer} < \gamma_{PS,P2VP}$). In turn, a lower BCP interface energy is favored by the system and is the reason for the MWCNT segregation to the BCP interface which is observed in the present study. This is basically the same situation as encountered in a Pickering emulsion, i.e., an emulsion stabilized by colloidal particles. A Pickering emulsion of the oil/water/CNT system has recently been described.[26,41] Even when the selective solvent (*p*-xylene, δ_{xylene} = 18.0 MPa$^{1/2}$)[38] for PS, used for micelle formation, is taken into account, the CNT solubility parameter still lies between the effective PS/solvent solubility parameter and that of the P2VP block.

Table 1. Hildebrand Solubility Parameters and Derived Quantities

	i		
	PS [(MPa)$^{1/2}$]	CNT [(MPa)$^{1/2}$]	P2VP [(MPa)$^{1/2}$]
δ_i	19.9[37,38] *a,b*	20.8[39] *b*	21.3[40]
$\lvert\delta_i - \delta_{PS}\rvert \sim \gamma_{i,PS}$	0	0.9	1.4
$\lvert\delta_i - \delta_{P2VP}\rvert \sim \gamma_{i,P2VP}$	1.4	0.5	0

[a]Arithmetic mean was used when multiple data were available. [b]When necessary, Hansen solubility parameters were converted to Hildebrand solubility parameters according to ref 38 (see Supporting Information for calculation).

In addition to the interfacial tension, which is sufficient to describe the energy in liquid/liquid interfaces, for the BCP interface, the chain stretching is another important contribution (second term, right-hand side of eq 1). The chain stretching also favors the MWCNT segregation to the BCP interface: Because of the chain stretching, the number of possible polymer chain conformations in the interface is reduced. Therefore, to place the MWCNT within one of the "bulk" phases has a higher entropic penalty than to place it within the interface. In Figure 6, this principle is visualized by a simple sketch where always the same number in chain conformations is represented by differently sized rectangles.

When the selective solvent is considered that renders the P2VP block impermeable and the PS block more flexible, the chain stretching within the interface will be even more pronounced and again leads to a MWCNT segregation to the BCP interface.

Since one can assume that the decrease in the BCP interface energy is maximized by the segregation of individual MWCNTs, the interface will not be crowded by agglomerated MWCNTs which may explain why only a wrapping by individual tubes is observed and also why BCPs are so effective to disperse MWCNTs: Especially BCP micelles offer a high area density of BCP interfaces.

We did not prove experimentally whether the MWCNT segregation to the BCP interface is a global energy minimum or a trapped state because both thermal annealing and solvent annealing are experimentally challenging. Both led to strong dewetting effects which prevented the observation in the TEM. Thus, we cannot experimentally rule out that the flow processes of the MWCNT/BCP micelles solution on the water surface, driven by the coalescence of colloidal micelles due to the capillary attraction, contributed to the development of the structure. Nevertheless, we conclude that the MWCNT segregation is mainly due to the thermodynamics considerations presented above because the absences of individual micelles in the film, i.e., the lack of a hard-sphere closed packed structure, suggests that any flow process of individual micelles

dx.doi.org/10.1021/la502298j | *Langmuir* 2014, 30, 14263−14269

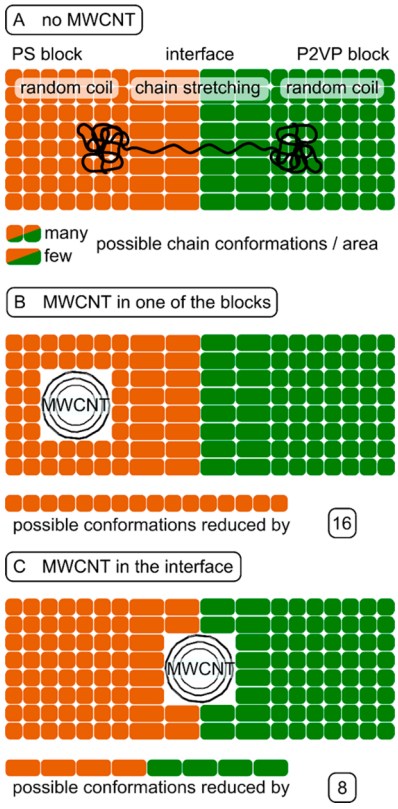

Figure 6. Sketch to demonstrate the entropic penalty to the free energy for placing a MWCNT in either one block or the interface of a BCP. Each rectangle represents the same amount of possible chain conformations. A low loss in possible chain conformations is entropically favored. (A) BCP without MWCNT. The possible chain conformations in the interface are reduced due to the chain stretching. (B) MWCNT placed within one of the blocks. (C) MWCNT placed within the BCP interface. The loss of possible conformations is lower within the interface. Therefore, the MWCNT segregation to the BCP interface is entropically favored.

must have been ceased before the corona became glassy to trap the MWCNT.

Since it is possible to grow CNTs of predetermined lengths,[42] the present study has the potential to enable the assembly of cost-effective flexible CNT-based metamaterials with MWCNT single split-ring resonators.[28,29] Another potential application are thin conductive nanocomposite films because the percolation threshold ought to be diminished dramatically if the MWCNTs are located at a small area fraction of the polymeric matrix only, yet are globally well dispersed. In addition, individual copolymer micelles can form complex shapes[21,43] and may be regularly arranged which opens the route to even more complex nanomaterials with unique properties by the presented copolymer micelle templating.

CONCLUSION

In conclusion, in the present study we report on the templating of MWCNT by BCP micelles benefiting simultaneously from the dispersibility of CNTs in amphiphilic copolymers and the nanostructure formation in selective solvents at the same time. The specific segregation is explained by the interfacial tension in the BCP interface and the chain entropy: The MWCNT segregation to the interface decreases the former and reduces the latter and is, thus, favorable. The templated MWCNT/copolymer nanocomposites may be applied in the future in nanooptics as metamerials or conductive films with extremely low percolation threshold. This study opens the route for a new generation of internal spatially arranged CNT/BCP nanocomposites where the properties of the CNTs are not adversely influenced by chemical modification.

ASSOCIATED CONTENT

Supporting Information

Unprocessed TEM micrographs; additional TEM micrographs of the MWCNT/BCP micelle thin film; additional TEM micrographs of BCP only; AFM image of the MWCNT/BCP micelle thin film's air−film interface; TEM micrograph of MWCNT agglomerate; description of the MWCNT location distribution determination; estimation of the MWCNT bending energy; definition of all terms in eq 1 and derivation of eq 2; conversion of Hansen to Hildebrandt solubility parameters. This material is available free of charge via the Internet at http://pubs.acs.org.

AUTHOR INFORMATION

Corresponding Author

*E-mail k.jandt@uni-jena.de; Tel +49 (0) 3641 94 77 30; Fax +49 (0) 3641 94 77 32 (K.D.J.).

Present Address

C.S.: Department of Materials, ETH Zurich, Wolfgang-Pauli-Strasse 10, 8093 Zurich, Switzerland.

Notes

The authors declare no competing financial interest.

REFERENCES

(1) Haggenmueller, R.; Fischer, J. E.; Winey, K. I. Single Wall Carbon Nanotube/Polyethylene Nanocomposites: Nucleating and Templating Polyethylene Crystallites. *Macromolecules* **2006**, *39*, 2964−2971.

(2) Cataldo, S.; Salice, P.; Menna, E.; Pignataro, B. Carbon Nanotubes and Organic Solar Cells. *Energy Environ. Sci.* **2012**, *5*, 5919−5940.

(3) Pradhan, B.; Setyowati, K.; Liu, H.; Waldeck, D. H.; Chen, J. Carbon Nanotube-Polymer Nanocomposite Infrared Sensor. *Nano Lett.* **2008**, *8*, 1142−1146.

(4) Ahir, S. V.; Terentjev, E. M. Photomechanical Actuation in Polymer-Nanotube Composites. *Nat. Mater.* **2005**, *4*, 491−495.

(5) Park, H.; Afzali, A.; Han, S.-J.; Tulevski, G. S.; Franklin, A. D.; Tersoff, J.; Hannon, J. B.; Haensch, W. High-Density Integration of Carbon Nanotubes via Chemical Self-Assembly. *Nat. Nanotechnol.* **2012**, *7*, 787−791.

(6) Banerjee, S.; Hemraj-Benny, T.; Wong, S. S. Covalent Surface Chemistry of Single-Walled Carbon Nanotubes. *Adv. Mater.* **2005**, *17*, 17−29.

(7) Moore, V. C.; Strano, M. S.; Haroz, E. H.; Hauge, R. H.; Smalley, R. E.; Schmidt, J.; Talmon, Y. Individually Suspended Single-Walled Carbon Nanotubes in Various Surfactants. *Nano Lett.* **2003**, *3*, 1379−1382.

(8) Nativ-Roth, E.; Shvartzman-Cohen, R.; Bounioux, C.; Florent, M.; Zhang, D.; Szleifer, I.; Yerushalmi-Rozen, R. Physical Adsorption of Block Copolymers to SWNT and MWNT: A Nonwrapping Mechanism. *Macromolecules* **2007**, *40*, 3676−3685.

(9) Shvartzman-Cohen, R.; Levi-Kalisman, Y.; Nativ-Roth, E.; Yerushalmi-Rozen, R. Generic Approach for Dispersing Single-Walled Carbon Nanotubes: The Strength of a Weak Interaction. *Langmuir* **2004**, *20*, 6085−6088.

(10) Park, C.; Lee, S.; Lee, J. H.; Lim, J.; Lee, S. C.; Park, M.; Lee, S.-S.; Kim, J.; Park, C. R.; Kim, C. Controlled Assembly of Carbon Nanotubes Encapsulated with Amphiphilic Block Copolymer. *Carbon* **2007**, *45*, 2072−2078.

(11) Kang, Y.; Taton, T. A. Micelle-Encapsulated Carbon Nanotubes: A Route to Nanotube Composites. *J. Am. Chem. Soc.* **2003**, *125*, 5650−5651.
(12) Shen, J.; Hu, Y.; Qin, C.; Li, C.; Ye, M. Dispersion Behavior of Single-Walled Carbon Nanotubes by Grafting of Amphiphilic Block Copolymer. *Composites, Part A* **2008**, *39*, 1679−1683.
(13) Shin, H.-I.; Min, B. G.; Jeong, W.; Park, C. Amphiphilic Block Copolymer Micelles: New Dispersant for Single Wall Carbon Nanotubes. *Macromol. Rapid Commun.* **2005**, *26*, 1451−1457.
(14) Arras, M. M. L.; Schillai, C.; Keller, T. F.; Schulze, R.; Jandt, K. D. Alignment of Multi-Wall Carbon Nanotubes by Disentanglement in Ultra-Thin Melt-Drawn Polymer Films. *Carbon* **2013**, *60*, 366−378.
(15) Ajayan, P. M.; Stephan, O.; Colliex, C.; Trauth, D. Aligned Carbon Nanotube Arrays Formed by Cutting a Polymer Resin-Nanotube Composite. *Science* **1994**, *265*, 1212−1214.
(16) Wode, F.; Tzounis, L.; Kirsten, M.; Constantinou, M.; Georgopanos, P.; Rangou, S.; Zafeiropoulos, N. E.; Avgeropoulos, A.; Stamm, M. Selective Localization of Multi-Wall Carbon Nanotubes in Homopolymer Blends and a Diblock Copolymer. Rheological Orientation Studies of the Final Nanocomposites. *Polymer* **2012**, *53*, 4438−4447.
(17) Li, Q.; Sun, J.; Wang, J.; Chen, G.-X.; Li, F.; Zhang, Y. Preparation of Diblock Copolymer Films for the Localization of C60 and Multiwalled Carbon Nanotubes on Aqueous Substrate. *RSC Adv.* **2012**, *2*, 6637−6644.
(18) Park, I.; Lee, W.; Kim, J.; Park, M.; Lee, H. Selective Sequestering of Multi-Walled Carbon Nanotubes in Self-Assembled Block Copolymer. *Sens. Actuators, B* **2007**, *126*, 301−305.
(19) Duque, D. Theory of Copolymer Micellization. *J. Chem. Phys.* **2003**, *119*, 5701−5704.
(20) Leibler, L.; Orland, H.; Wheeler, J. C. Theory of Critical Micelle Concentration for Solutions of Block Copolymers. *J. Chem. Phys.* **1983**, *79*, 3550−3557.
(21) Wen, G.; Chung, B.; Chang, T. Effect of Spreading Solvents on Langmuir Monolayers and Langmuir-Blodgett Films of PS-b-P2VP. *Polymer* **2006**, *47*, 8575−8582.
(22) Cox, J. K.; Yu, K.; Constantine, B.; Eisenberg, A.; Lennox, R. B. Polystyrene-Poly(ethylene oxide) Diblock Copolymers Form Well-Defined Surface Aggregates at the Air/Water Interface. *Langmuir* **1999**, *15*, 7714−7718.
(23) Chen, D.; Zhao, W.; Wei, D.; Russell, T. P. Dewetting on Curved Interfaces: A Simple Route to Polymer Nanostructures. *Macromolecules* **2011**, *44*, 8020−8027.
(24) Zou, S.; Maspoch, D.; Wang; Mirkin, C. A.; Schatz, G. C. Rings of Single-Walled Carbon Nanotubes: Molecular-Template Directed Assembly and Monte Carlo Modeling. *Nano Lett.* **2007**, *7*, 276−280.
(25) Hinds, B. J.; Chopra, N.; Rantell, T.; Andrews, R.; Gavalas, V.; Bachas, L. G. Aligned Multiwalled Carbon Nanotube Membranes. *Science* **2004**, *303*, 62−65.
(26) Wang, W.; Laird, E. D.; Gogotsi, Y.; Li, C. Y. Bending Single-Walled Carbon Nanotubes into Nanorings Using a Pickering Emulsion-Based Process. *Carbon* **2012**, *50*, 1769−1775.
(27) Sano, M.; Kamino, A.; Okamura, J.; Shinkai, S. Ring Closure of Carbon Nanotubes. *Science* **2001**, *293*, 1299−1301.
(28) Klein, M. W.; Enkrich, C.; Wegener, M.; Soukoulis, C. M.; Linden, S. Single-Slit Split-Ring Resonators at Optical Frequencies: Limits of Size Scaling. *Opt. Lett.* **2006**, *31*, 1259−1261.
(29) Ramakrishna, S. A. Physics of Negative Refractive Index Materials. *Rep. Prog. Phys.* **2005**, *68*, 449−521.
(30) Hobbie, E. K.; Fagan, J. A.; Obrzut, J.; Hudson, S. D. Microscale Polymer-Nanotube Composites. *ACS Appl. Mater. Interfaces* **2009**, *1*, 1561−1566.
(31) Bronstein, L. M.; Sidorov, S. N.; Valetsky, P. M.; Hartmann, J.; Cölfen, H.; Antonietti, M. Induced Micellization by Interaction of Poly(2-vinylpyridine)-*block*-poly(ethylene oxide) with Metal Compounds. Micelle Characteristics and Metal Nanoparticle Formation. *Langmuir* **1999**, *15*, 6256−6262.
(32) Bockstaller, M. R.; Lapetnikov, Y.; Margel, S.; Thomas, E. L. Size-Selective Organization of Enthalpic Compatibilized Nanocrystals in Ternary Block Copolymer/Particle Mixtures. *J. Am. Chem. Soc.* **2003**, *125*, 5276−5277.
(33) Thompson, R. B.; Ginzburg, V. V.; Matsen, M. W.; Balazs, A. C. Predicting the Mesophases of Copolymer-Nanoparticle Composites. *Science* **2001**, *292*, 2469−2472.
(34) He, L.; Zhang, L.; Liang, H. Mono- or Bidisperse Nanorods Mixtures in Diblock Copolymers. *Polymer* **2010**, *51*, 3303−3314.
(35) Jin, J.; Wu, J. A Theoretical Study for Nanoparticle Partitioning in the Lamellae of Diblock Copolymers. *J. Chem. Phys.* **2008**, *128*, 074901−1−074901−9.
(36) Bates, F. S.; Fredrickson, G. H. Block Copolymers − Designer Soft Materials. *Phys. Today* **1999**, *52*, 32−38.
(37) DiPaola-Baranyi, G.; Guillet, J. E. Estimation of Polymer Solubility Parameters by Gas Chromatography. *Macromolecules* **1978**, *11*, 228−235.
(38) Hansen, C. M. *Hansen Solubility Parameters: A User's Handbook*, 1st ed.; CRC Press: Boca Raton, FL, 1999.
(39) Bergin, S. D.; Sun, Z.; Rickard, D.; Streich, P. V.; Hamilton, J. P.; Coleman, J. N. Multicomponent Solubility Parameters for Single-Walled Carbon Nanotube-Solvent Mixtures. *ACS Nano* **2009**, *3*, 2340−2350.
(40) Arichi, S.; Matsuura, H.; Tanimoto, Y.; Murata, H. Studies of Poly-2-vinylpyridine. II. Solubilities in Various Solvents. *Bull. Chem. Soc. Jpn.* **1966**, *39*, 434−439.
(41) Feng, T.; Hoagland, D. A.; Russell, T. P. Assembly of Acid-Functionalized Single-Walled Carbon Nanotubes at Oil/Water Interfaces. *Langmuir* **2014**, *30*, 1072−1079.
(42) Puretzky, A. A.; Geohegan, D. B.; Jackson, J. J.; Pannala, S.; Eres, G.; Rouleau, C. M.; More, K. L.; Thonnard, N.; Readle, J. D. Incremental Growth of Short SWNT Arrays by Pulsed Chemical Vapor Deposition. *Small* **2012**, *8*, 1534−1542.
(43) Kinning, D. J.; Winey, K. I.; Thomas, E. L. Structural Transitions from Spherical to Nonspherical Micelles in Blends of Poly(styrene-butadiene) Diblock Copolymer and Polystyrene Homopolymers. *Macromolecules* **1988**, *21*, 3502−3506.